TOPS: New DOA Estimator for Wideband Signals

Yeo-Sun Yoon, *Member, IEEE*, Lance M. Kaplan, *Senior Member, IEEE*, and James H. McClellan, *Fellow, IEEE*

***Abstract*—This paper introduces a new direction-of-arrival (DOA) estimation algorithm for wideband sources called test of orthogonality of projected subspaces (TOPS). This new technique estimates DOAs by measuring the orthogonal relation between the signal and the noise subspaces of multiple frequency components of the sources. TOPS can be used with arbitrary shaped one-dimensional (1-D) or two-dimensional (2-D) arrays. Unlike other coherent wideband methods, such as the coherent signal subspace method (CSSM) and WAVES, the new method does not require any preprocessing for initial values. The performance of those wideband techniques and incoherent MUSIC is compared with that of the new method through computer simulations. The simulations show that this new technique performs better than others in mid signal-to-noise ratio (SNR) ranges, while coherent methods work best in low SNR and incoherent methods work best in high SNR. Thus, TOPS fills a gap between coherent and incoherent methods.**

***Index Terms*—Array signal processing, direction-of-arrival (DOA) estimation, signal subspace method, wideband sources.**

I. Introduction

THE number of radar, sonar, and wireless communication applications requiring the localization of a signal source is ever increasing. Direction-of-arrival (DOA) estimation using data collected from an array of antennas/sensors is the primary signal processing technology supporting these applications [1]. Consequently, many DOA methods have been proposed in an effort to improve estimation performance and/or computational efficiency. Maximum-likelihood (ML) methods and signal subspace methods are examples of those. Many of the DOA methods are applicable only to narrowband signal sources. The energy of narrowband signals are concentrated in a frequency band that is relatively small compared with the center (carrier) frequency. As a result, the sensor output can be easily vectorized by using just one frequency component, i.e., the center frequency of the sources. The sensor output vector forms a vector space, and this is the main idea of the signal subspace methods. The vector space can be found by exploiting the spatial correlation matrix of the sensor output. The reason why we cannot apply narrowband signal subspace methods to wideband sources is that the phase difference between sensor outputs is no longer just dependent on the DOA alone, but also depends on the temporal frequency, which has a wide range. One intuitive method that one can easily formulate for wideband processing is to decompose the wideband signal into many narrowband signals with the discrete Fourier transform (DFT), or equivalently with a filter bank that consists of identical nonoverlapping bandpass filters. The DFT decomposition provides a set of narrowband signals of different frequencies and the corresponding correlation matrices. Wideband DOA estimation is a matter of using these multiple correlation matrices *wisely* so that the DOA estimator works better than any narrowband method using only one frequency. This problem is applicable to any signal whose energy is not concentrated in a narrow bandwidth, e.g., acoustic sources composed of multiple harmonics due to vehicle engines or helicopter propellers [2].

In some favorable situations [e.g., high signal-to-noise ratio (SNR), well-separated sources, or many sensors], the narrowband methods that use only one frequency component are good enough for estimation. However, in many cases, using information from multiple frequency bins in a wideband method is necessary to achieve the processing gain needed to obtain good estimates.

Recently, applications where wideband signals are favored over narrowband signals are receiving more attention. These applications are driving the need for better wideband DOA estimation. The incoherent signal subspace method (ISSM) is one of the simplest wideband methods. It passes the sensor output through a filter bank to decompose the wideband sources into narrowband ones and then applies narrowband techniques, such as MUSIC [3], independently to the outputs from the filter bank. Then, the results from all the frequency bins are averaged to get the final DOA estimate. Although ISSM is simple and effective in high-SNR cases, it suffers when the SNR at each frequency varies, because the DOA estimate at some frequencies could be very bad. A single outlier could spoil the final estimates in the averaging process. In order to overcome such disadvantages, a number of improved methods have been proposed [4]–[10]. Among those are the coherent signal subspace method (CSSM) [4] and weighted average of signal subspaces (WAVES) [5]. CSSM requires initial values to find focusing matrices, and the estimation performance of CSSM is sensitive to these initial values. In fact, poor initial values can lead to biased estimates [11]. WAVES also requires focusing matrices. Although it can avoid the initial-value requirement by using a

Manuscript received October 24, 2004; revised June 17, 2005. Prepared through collaborative participation in the Advanced Sensors Consortium sponsored by the U. S. Army Research Laboratory under the Collaborative Technology Alliance Program, Cooperative Agreement DAAD19-01-2-0008. The U.S. Government is authorized to reproduce and distribute reprints for Government purposes notwithstanding any copyright notation thereon. The views and conclusions contained in this document are those of the authors and should not be interpreted as representing the official policies, either expressed or implied, of the Army Research Laboratory or the U. S. Government. The associate editor coordinating the review of this manuscript and approving it for publication was Prof. Alex B. Gershman.

Y.-S. Yoon is with the Samsung Thales Company, Ltd., Yongin 449-885, Korea (e-mail: yeosun.yoon@samsung.com).

L. M. Kaplan is with the U. S. Army Research Laboratory, Adelphi, MD 20783 USA (e-mail: lkaplan@arl.army.mil).

J. H. McClellan is with the Center for Signal and Image Processing (CSIP), School of Electrical and Computer Engineering, Georgia Institute of Technology, Atlanta, GA 30318 USA (e-mail: jim.mcclellan@ece.gatech.edu).

Digital Object Identifier 10.1109/TSP.2006.872581

beamforming invariance technique [8], its performance is worse than when it uses focusing matrices with good initial values like CSSM [5] and the existence of the beamforming matrix depends on the size of a field of view (FOV) and the array geometry. The effect of the focusing angles on the estimator has not received much attention in the literature [11].

In this paper, we propose a new wideband signal subspace DOA estimator called test of orthogonality of projected subspaces (TOPS). Unlike coherent methods that must align the signal and noise subspaces to form a viable general covariance matrix, TOPS determines whether or not a DOA dependent transformation is able to achieve the alignment. Although TOPS does not cohere the subspaces over frequency to achieve processing gain, the multiple alignment test over frequency bins leads to a more robust estimator at lower SNR than incoherent methods. The advantages of TOPS are 1) it does not require focusing angles or beamforming matrix, 2) it does not suffer from bias at large SNR, and 3) at low SNR, it better integrates frequency bins than incoherent methods.

This paper is organized as follows. In Section II, some of the previously proposed wideband methods are reviewed. The new approach is explained in Section III followed by Section IV where simulation results are shown. Finally, Section V concludes this paper.

II. Previous Wideband Subspace Methods

A. Signal Model

Let's consider an M-sensor linear array in which the sensors are not necessarily uniformly spaced, but we do assume that the array manifolds of different DOAs are independent. In other words, $P(\leq M)$ array manifolds with P different DOAs should span a P-dimensional subspace. Assume that the number of signal sources P is either known or can be estimated [4], [12]. The bandwidths of the wideband sources need not be identical, but there should be some frequency band $[\omega_L, \omega_H]$ where all the sources' bandwidths overlap. Then, the mth sensor output $x_m(t)$ is

$$x_m(t) = \sum_{l=0}^{P-1} s_l(t - \upsilon_m \sin\theta_l) + n_m(t) \tag{1}$$

where $s_l(t)$ is the lth signal source, $n_m(t)$ is noise at the mth sensor and $\upsilon_m = d_m/c$, where d_m is the distance between the mth sensor and the reference sensor, and c is the speed of the signal propagation. For uniform linear arrays (ULA), $\upsilon_m = md/c$, where d is sensor displacement. The angle θ_l is the DOA to be estimated. The noise $n_m(t)$ is assumed to be uncorrelated with the signal sources and white both temporally and spatially. Suppose that the observation time is long enough so that the Fourier transform of the sensor output has good resolution. The discrete-time Fourier transform (DTFT) of the mth sensor output is

$$X_m(\omega) = \sum_{l=0}^{P-1} S_l(\omega)\exp(-j\omega\upsilon_m \sin\theta_l) + N_m(\omega). \tag{2}$$

Most wideband subspace methods decompose the sensor outputs into several narrowband signals using a filter bank or the DFT. If the intersection of the frequency bands of all sources is $[\omega_L, \omega_H]$, then the output of the filter bank or DFT module can be written in vector form at K frequencies, as follows:

$$\mathbf{X}(\omega_i) = \mathbf{A}(\omega_i, \boldsymbol{\theta})\mathbf{S}(\omega_i) + \mathbf{N}(\omega_i), \quad i = 0, 1, \ldots, K-1 \tag{3}$$

where

$$\mathbf{X}(\omega_i) = [X_0(\omega_i) \quad X_1(\omega_i) \quad \cdots \quad X_{M-1}(\omega_i)]^T \tag{4}$$

$$\mathbf{S}(\omega_i) = [S_0(\omega_i) \quad S_1(\omega_i) \quad \cdots \quad S_{P-1}(\omega_i)]^T \tag{5}$$

$\omega_L < \omega_i < \omega_H$ for $i = 0, 1, 2, \ldots, K-1$, $\mathbf{A}(\omega_i, \boldsymbol{\theta})$ is the $M \times P$ steering matrix

$$\mathbf{A}(\omega_i, \boldsymbol{\theta}) = [\mathbf{a}(\omega_i, \theta_0)\ \mathbf{a}(\omega_i, \theta_1)\ \ldots\ \mathbf{a}(\omega_i, \theta_{P-1})] \tag{6}$$

whose columns are the $M \times 1$ array manifolds $\mathbf{a}(\omega_i, \theta_l)$ at frequency ω_i, i.e.,

$$\mathbf{a}(\omega_i, \theta_l) = [1\ e^{-j\omega_i \upsilon_1 \sin\theta_l}\ \ldots\ e^{-j\omega_i \upsilon_{M-1} \sin\theta_l}]^T \tag{7}$$

$\boldsymbol{\theta} = [\theta_0 \theta_1 \ldots \theta_{P-1}]^T$, and θ_l is the DOA of the lth source. Note that the first sensor serves as the reference sensor. For notational convenience, from now on, $\mathbf{A}(\omega_i, \boldsymbol{\theta})$ and $\mathbf{a}(\omega_i, \theta_j)$ will be represented as $\mathbf{A}_i(\boldsymbol{\theta})$ and $\mathbf{a}_i(\theta_j)$, respectively. The correlation matrix used in all signal subspace methods is

$$\mathbf{R}_i = E\left[\mathbf{x}_i \mathbf{x}_i^H\right] = \mathbf{A}_i \mathbf{R}_{ss}(\omega_i)\mathbf{A}_i^H + \sigma^2 \mathbf{I} \tag{8}$$

where the superscript H denotes conjugate transpose, and

$$\mathbf{R}_{ss}(\omega_i) = E\left[\mathbf{s}(\omega_i)\mathbf{s}^H(\omega_i)\right]. \tag{9}$$

If we assume that the P sources are uncorrelated so that the $P \times P$ matrix $\mathbf{R}_{ss}$ has full rank, then the signal subspace matrix $\mathbf{F}_i$ and the noise subspace matrix $\mathbf{W}_i$ at frequency ω_i can be formed from the eigenvalue decomposition (EVD) of the correlation matrix as

$$\mathbf{F}_i = [\mathbf{y}_{i,1}\ \mathbf{y}_{i,2}\ \ldots\ \mathbf{y}_{i,P}] \tag{10}$$

$$\mathbf{W}_i = [\mathbf{y}_{i,P+1}\ \mathbf{y}_{i,P+2}\ \ldots\ \mathbf{y}_{i,M}] \tag{11}$$

where $\mathbf{y}_{i,1}, \ldots, \mathbf{y}_{i,M}$ are the orthogonal eigenvectors of $\mathbf{R}_i$ indexed in descending order with respect to their corresponding eigenvalues. The range of the signal subspace $\mathbf{F}_i$ is equivalent to the range of $\mathbf{A}_i(\boldsymbol{\theta})$.

B. Incoherent Methods

As mentioned in the previous section, ISSM applies narrowband signal subspace methods to each $\mathbf{X}(\omega_i)$ independently. The estimated DOAs from each frequency bin are averaged in some way to give the final result [13], [14]. For example, if MUSIC is used as a narrowband method, the wideband DOA estimate is

$$\hat{\theta} = \arg\min_{\theta} \sum_{i=0}^{K-1} \mathbf{a}_i^H(\theta)\mathbf{W}_i\mathbf{W}_i^H\mathbf{a}_i(\theta) \tag{12}$$

where $\mathbf{W}_i$ is the noise subspace at frequency ω_i. The noise subspace matrix $\mathbf{W}_i$ is estimated from the spatial correlation matrix $\mathbf{R}_i$ in (8). Since the final estimates are averages of magnitude squared functions from different signal subspaces, ISSM is called an *incoherent* subspace method.

C. Coherent Methods

After ISSM, many methods have been proposed to find a good way to combine the sinal subspaces *coherently* into one general correlation matrix to which narrowband high-resolution methods can be applied. CSSM, proposed by Wang and Kaveh, was the first approach to sum the correlation matrices of various frequency bins coherently [4]. It transforms the correlation matrices at many frequency bins into one general correlation matrix at one focusing frequency by using a transformation matrix (focusing matrix) that depends on the frequency bin. This procedure is called *focusing*. The general procedure of coherent methods is

1) Determine focusing matrices, $\mathbf{T}_i$ for $i = 1, \ldots, K-1$, that transform the array manifolds for frequency i into corresponding array manifolds for frequency 0, i.e., the reference frequency. Note that $\mathbf{T}_0 = \mathbf{I}$.
2) Calculate the general correlation matrix as
$$\mathbf{R}_{\text{gen}} = \sum_{i=0}^{K-1} \alpha_i \mathbf{T}_i \mathbf{Q}_i \mathbf{T}_i^H \tag{13}$$
where α_i is a weighting and $\mathbf{Q}_i$ is a narrowband estimate of the correlation matrix.
3) Estimate DOA with narrowband signal subspace methods such as MUSIC using $\mathbf{R}_{\text{gen}}$ and $\mathbf{a}_0(\theta)$.

A focusing matrix attempts to cohere an array manifold corresponding to a given DOA at one frequency to the array manifold for that same DOA at a reference frequency. Ideally, the focusing matrix should work for the entire range of possible DOA values. In many array geometries, the ideal focusing matrix can not be achieved. Furthermore, the matrix should be approximately unitary. Otherwise, the singular values corresponding to the noise subspace could be amplified relative to those of the signal subspace. Then, the estimation algorithms may begin to confuse part of the noise subspace for the signal subspace.

For standard CSSM, the estimated narrowband correlations matrices are the sampled correlation matrices, i.e., $\mathbf{Q}_i = \mathbf{R}_i$ and the focusing matrices are unitary, i.e., $\mathbf{T}_i^H \mathbf{T}_i = \mathbf{I}$. Furthermore, the focusing matrices are designed to cohere manifolds as well as possible for a finite set of DOAs, which are referred to as *focusing angles*. To this end, the focusing matrices are designed to minimize a Frobenius norm for the manifold errors

$$\min_{\mathbf{T}_i} \|\mathbf{A}_0(\boldsymbol{\theta}_f) - \mathbf{T}_i \mathbf{A}_i(\boldsymbol{\theta}_f)\|_F \tag{14}$$

where ω_0 is the reference (or focusing) frequency and $\boldsymbol{\theta}_f$ is the set of focusing angles. The matrix $\mathbf{T}_i$ is known as the rotational signal subspace (RSS) focusing matrix [15]. RSS matrices are within the class of signal subspace transformation (SST) matrices that are well-known for their optimality in terms of preserving SNR after focusing [16].

CSSM can demonstrate better performance than ISSM, and by the averaging process in (13), it can deal with correlated sources [4]. However, the focusing matrices depend on the focusing angles, so preprocessing must be done to obtain "good" focusing angles that are close enough to the true DOAs. Even though the focusing direction might be very close to the true DOA, if it is not identical to the true DOA and if the focusing frequency is not the centroid of the signal's band, the bias will never go to zero [11].

The focusing matrix can easily be designed to perfectly cohere a single DOA. For example the unitary matrix

$$\mathbf{T}_i = \text{diag}\left\{e^{j(\omega_i - \omega_0)v_0 \sin(\theta_f)}, \ldots, e^{j(\omega_i - \omega_0)v_{M-1} \sin(\theta_f)}\right\} \tag{15}$$

is such a matrix. It represents a solution to (14) when the set of focusing angles only include θ_f. It can be shown that when this focusing matrix is used to generate $\mathbf{R}_{\text{gen}}$, good DOA estimation is possible within a local region around the focusing DOA θ_f [17]. This fact is the motivation of the steered covariance method (STCM) [17]. In STCM, the DOA space is partitioned, the focusing matrices are designed to focus around a single DOA representing the center of the partition, and CSSM is applied to each partition using the corresponding DOA center. STCM avoids the need for preprocessing to obtain prior estimates of the DOAs. The accuracy of STCM is proportional to the number of partitions used.

The need for preprocessing can also be circumvented by an alternative design of the focusing matrices. For example, the beamforming invariance CSSM (BICSSM) method is similar to CSSM in that $\mathbf{Q}_i = \mathbf{R}_i$, but (14) is not used to generate the focusing matrices [8]. Instead, the focusing matrices are designed to approximately cohere over a continuous range of DOAs, i.e., a FOV. The focusing matrices can be viewed as a set of beamformers. A reference set of beamformers are used to define $\mathbf{T}_0$, and these beamformers span the FOV. The beamformers for the other frequencies are designed to minimize the "average" error metric over the FOV between the beamformed responses of frequency i and the reference frequency. For the focusing matrices to be effective, the reference beamformers comprising $\mathbf{T}_0$ should demonstrate low sidelobes outside the FOV. Furthermore, the beam patterns should be invariant between the frequency components. Sophisticated metrics to design such focusing matrices appear in [5]. Unfortunately, when the FOV is too wide, the ability of BICSSM to cohere the subspaces from different frequency bins is severely diminished. In other words, when no preprocessing is exploited to obtain prior information about the DOAs, the effectiveness of BICSSM can be poor in comparison to CSSM.

The array manifold interpolation (AMI) is another interesting technique that can avoid preprocessing [6], [18]. Again, $\mathbf{Q}_i = \mathbf{R}_i$ and the focusing matrices are designed to work over a wide range of DOAs. In AMI, the focusing matrices are designed to minimize the maximum error between the focused and reference manifolds over the range of possible DOA values. Through infinite dimensional linear decomposition of the array manifold, it may be possible for the maximum error to be arbitrarily small over the full 360° range of DOAs [18]. As a result, one might be able to generate the focusing matrix without any prior information about the DOAs. However, for many array geometries, the maximum focusing error can only become arbitrarily small over a narrow range of DOAs. Furthermore, the focusing matrices are not unitary so that part of the noise subspace can be confused as signal subspace.

WAVES is one of the latest signal subspace methods [5]. One of the main differences from previous methods is that it does not use $\mathbf{Q}_i = \mathbf{R}_i$ in (13). Instead it uses weighted signal subspaces [19]. That is

$$\mathbf{Q}_i = \mathbf{F}_i \mathbf{P}_i \mathbf{P}_i^H \mathbf{F}_i^H \tag{16}$$

where $\mathbf{F}_i$ is the signal subspace, and $\mathbf{P}_i$ is the weighting matrix of frequency ω_i. The focusing matrix can be determined by any method, e.g., RSS, BICSSM. The weighting matrix $\mathbf{P}_i$ is from [19].

By weighting the signal subspace and removing the noise subspace at each frequency bin, WAVES is more robust than CSSM-like methods, i.e., $\mathbf{Q}_i = \mathbf{R}_i$, at moderate SNR.

Overall, the estimation performance of the coherent methods depends on the chosen focusing matrices. When the initial DOA estimates are good, the RSS matrices will lead to better estimation accuracy than focusing matrices that attempt to cohere over a large range of DOAs [5]. Therefore, we only consider RSS focusing matrices for the remainder of this paper.

III. TOPS Method

This section introduces a new wideband DOA estimation method. We name the new method *test of orthogonality of projected subspaces* (TOPS). The following subsections describe the theory, structure and computational complexity of the algorithm.

A. Theory

Similar to the previous wideband methods, TOPS uses the DFT of sensor outputs, which are described by the array model in (3). Initially, we will consider linear arrays with arbitrary sensor locations, along with the additional constraint that the array manifolds of different DOAs should be independent. Later, multidimensional arrays will be considered. Like CSSM and WAVES, TOPS also uses a transformation matrix to exploit multiple frequency components. However, TOPS does not use the transformation matrix to generate the general correlation matrix $\mathbf{R}_{\text{gen}}$. Because the focusing matrices do not cohere the DOAs perfectly over the FOV, the methods discussed in Section II-C will not lead to perfect estimates in the absence of noise. On the other hand, TOPS can provide perfect measurements for infinite SNR. Like STCM, TOPS uses the RSS matrices designed for a single DOA. However, it uses the transformation matrix at each hypothesized DOA to perform an orthogonality test between the transformed signal subspace and the noise subspace. If the hypothesized DOA corresponds to a true DOA, then orthogonality is preserved; otherwise, it is not.

TOPS uses a diagonal unitary transformation matrix, similar to STCM (see (15)). Specifically, the kth term on the diagonal of the transformation matrix $\mathbf{\Phi}(\omega_i, \theta_i)$ is

$$[\mathbf{\Phi}(\omega_i, \theta_i)]_{(k,k)} = \exp(-j\omega_i v_k \sin\theta_i). \tag{17}$$

The transformation matrix is able to preserve the array manifolds as shown in the following lemma.

Lemma 1: Given a linear array manifold $\mathbf{a}_i(\theta_i)$, and a matrix $\mathbf{\Phi}(\omega_j, \theta_j)$, the product is a new array manifold

$$\mathbf{a}_k(\theta_k) = \mathbf{\Phi}(\omega_j, \theta_j)\mathbf{a}_i(\theta_i) \tag{18}$$

where the relations between frequencies and DOAs are

$$\omega_k = \omega_i + \omega_j, \tag{19}$$

$$\sin\theta_k = \frac{\omega_i}{\omega_k}\sin\theta_i + \frac{\omega_j}{\omega_k}\sin\theta_j. \tag{20}$$

Proof: The matrix multiplication in (18) is actually a phase shift of the elements of the array manifold, so we obtain

$$\begin{aligned}[\mathbf{\Phi}(\omega_j, \theta_j)\mathbf{a}_i(\theta_i)]_p &= e^{-j\omega_j v_{p-1}\sin\theta_j} \cdot e^{-j\omega_i v_{p-1}\sin\theta_i} \\ &= e^{-jv_{p-1}(\omega_i+\omega_j)\left(\frac{\omega_i}{\omega_i+\omega_j}\sin\theta_i + \frac{\omega_j}{\omega_i+\omega_j}\right)}\end{aligned} \tag{21}$$

where $[\cdot]_p$ denotes the pth element of the vector. Using (19) and (20), we can rewrite (21) as

$$[\mathbf{\Phi}(\omega_j, \theta_j)\mathbf{a}_i(\theta_i)]_p = e^{-j\omega_k v_{p-1}\sin\theta_k} \tag{22}$$

$$= [\mathbf{a}_k(\theta_k)]_p. \tag{23}$$

Since $|\omega_i \sin\theta_i + \omega_j \sin\theta_j| \le \omega_k$, the expression for $\sin\theta_k$ is legitimate. ■

This lemma demonstrates that one can transform an array manifold at any given frequency and DOA into another array manifold corresponding to a desired frequency through matrix multiplication via $\mathbf{\Phi}(\omega, \theta)$. Although the proof assumes that the sensor gains are unity, it is easy to show that the lemma holds for different gains as long as the relative sensor gains are consistent over the frequency bins. Otherwise, the transformation matrix must be designed with knowledge of the relative gains for each frequency bins. The case of nonunity sensor gains is beyond the scope of this paper.

Note that if $\theta_i = \theta_j$, then $\theta_k = \theta_i$ so that it is possible to transform the array manifold of one frequency into that of another frequency without changing the DOA. This is a key component of the TOPS algorithm.

Lemma 2: Let $\Delta\omega = \omega_j - \omega_i$. Then, the following two range spaces are identical:

$$\mathcal{R}\{\mathbf{\Phi}(\Delta\omega, \phi)\mathbf{F}_i\} = \mathcal{R}\left\{\mathbf{A}(\omega_j, \hat{\boldsymbol{\theta}})\right\} \tag{24}$$

where the new angles $\hat{\boldsymbol{\theta}}$ depend on ϕ in the following manner:

$$[\hat{\boldsymbol{\theta}}]_i = \arcsin\left\{\frac{\omega_i}{\omega_j}\sin\theta_i + \frac{\Delta\omega}{\omega_j}\sin\phi\right\} \tag{25}$$

Proof: Since the range spaces of $\mathbf{F}_i$ and $\mathbf{A}_i(\boldsymbol{\theta})$ are identical, there exists a full-rank square matrix $\mathbf{G}_i$ such that $\mathbf{F}_i = \mathbf{A}_i(\boldsymbol{\theta})\mathbf{G}_i$. By Lemma 1, we can easily show that

$$\begin{aligned}\mathbf{\Phi}(\Delta\omega, \phi)\mathbf{F}_i &= \mathbf{\Phi}(\Delta\omega, \phi)\mathbf{A}_i(\boldsymbol{\theta})\mathbf{G}_i \\ &= \mathbf{A}_j(\hat{\boldsymbol{\theta}})\mathbf{G}_i\end{aligned} \tag{26}$$

which confirms the equality of the range spaces. ■

Now we show that it is possible to formulate a test in which the rank of a matrix decreases when the angle ϕ in the transformation matrix $\mathbf{\Phi}(\Delta\omega_i, \phi)$ of Lemma 2 equals one of the angles in the steering matrix $\mathbf{A}_i(\boldsymbol{\theta})$. This is the core of the TOPS algorithm.

Theorem: Assume that $2P \leq M$ and $K \geq P+1$. Let's define the $M \times P$ matrices $\mathbf{U}_i(\phi)$ as

$$\mathbf{U}_i(\phi) = \mathbf{\Phi}(\Delta\omega_i, \phi)\mathbf{F}_0, \qquad i = 1, \ldots, K-1 \tag{27}$$

where $\Delta\omega_i = \omega_i - \omega_0$, and ϕ is a hypothesized azimuth angle.[1] Define a $P \times (K-1)(M-P)$ matrix $\mathbf{D}(\phi)$ as

$$\mathbf{D}(\phi) = \left[\mathbf{U}_1^H \mathbf{W}_1 | \mathbf{U}_2^H \mathbf{W}_2 | \ldots | \mathbf{U}_{K-1}^H \mathbf{W}_{K-1}\right]. \tag{28}$$

Then the following applies:

a) if $\phi = \theta_l$ for some l, $\mathbf{D}(\phi)$ loses its rank (becomes rank-deficient);
b) if $\mathbf{D}(\phi)$ is full rank matrix, $\phi \neq \theta_l$ for all l.

Proof: See Appendix A. ∎

This theorem holds as long as the source signals are not fully correlated. In other words, TOPS works when the dimension of the $\mathbf{F}_i$ is the same as that of the signal subspace for all i. However, when some of the sources are fully correlated, the dimensionality of the signal subspace decreases and like the performance of most DOA estimators, the performance of TOPS degrades.

B. Extension to Arbitrary Multidimensional Arrays

In the previous section, TOPS was applied to linear one-dimensional (1-D) arrays. In this section, it is generalized for the case of arbitrarily shaped multidimensional arrays. Even though we say *arbitrary* arrays, we need the conditions that the array manifold vectors of different DOAs be mutually independent, and that the distance between sensors be small enough to avoid spatial aliasing. In order to derive TOPS to work with arbitrary arrays, the following two conditions should hold:

1) there always exists a transformation matrix such as $\mathbf{\Phi}(\omega, \phi)$ in (18);
2) the $\mathbf{D}(\phi)$ matrix should be full rank unless ϕ is equal to one of the DOAs.

If condition 1) is satisfied, then condition 2) will also be satisfied since we assume that the array manifolds of different DOAs are linearly independent. Although the relation (20) will be slightly different depending on the array shape, if the matrix $\mathbf{\Phi}(\omega, \phi)$ exists, the TOPS estimator will work.

For arbitrary arrays, we need to redefine the array manifold vector so that the mth element of the array manifold vector is

$$\exp\{-j\omega\vec{\alpha} \cdot \vec{x}_m\} \tag{29}$$

where the exponent involves the three-dimensional (3-D) dot product between $\vec{x}_m$, the 3-D position vector of the mth sensor, and $\vec{\alpha}$, the slowness vector, where

$$\vec{\alpha} = \frac{1}{c}(\sin\theta\sin\varphi, \cos\theta\sin\varphi, \cos\varphi) \tag{30}$$

with θ and φ being the azimuth and elevation angles, respectively [20]. Note that the magnitude of a slowness vector is always $|\vec{\alpha}| = 1/c$. The array manifold for the linear array in (7) is a special case of this general array manifold.

[1]The angle ϕ is not the elevation angle used for two-dimensional (2-D) arrays; we will use φ for the elevation angle.

In this general case, we define the transformation matrix $\mathbf{\Phi}$ as

$$[\mathbf{\Phi}(\omega, \vec{\alpha})]_{(k,k)} = \exp\{-j\omega(\vec{\alpha} \cdot \vec{x}_k)\} \tag{31}$$

and then we examine the transformed array manifold to see if it is also an array manifold. If the vector $\mathbf{b}$ denotes the transformed array manifold

$$\mathbf{b} = \mathbf{\Phi}(\omega_a, \vec{\alpha}_a)\mathbf{a}(\omega_b, \vec{\alpha}_b). \tag{32}$$

We would like to show that the phase of the mth element of $\mathbf{b}$ can be written in the form

$$b_m = \omega_c\vec{\beta} \cdot \vec{x}_m = \omega_a\vec{\alpha}_a \cdot \vec{x}_m + \omega_b\vec{\alpha}_b \cdot \vec{x}_m \tag{33}$$

where $\omega_c = \omega_a + \omega_b$ and $\vec{\beta}$ is a legitimate slowness vector, i.e., its magnitude is $1/c$.

There are three cases to consider depending on whether the set of sensor positions $\{\vec{x}_m\}$ spans one, two or three dimensions. When the span is three-dimensional, simple algebra leads to the following expression for $\vec{\beta}$:

$$\begin{aligned}\vec{\beta} &= \frac{\omega_a\vec{\alpha}_a + \omega_b\vec{\alpha}_b}{\omega_c} \\ &= \zeta\vec{\alpha}_a + (1-\zeta)\vec{\alpha}_b\end{aligned} \tag{34}$$

where $\zeta = \omega_a/\omega_c$. Since $\vec{\alpha}_a$ and $\vec{\alpha}_b$ are slowness vectors, their magnitude equals $1/c$, so the triangle inequality gives

$$|\vec{\beta}| \leq \zeta|\vec{\alpha}_a| + (1-\zeta)|\vec{\alpha}_b| = \frac{1}{c}. \tag{35}$$

Equality holds if and only if $\vec{\alpha}_a$ is proportional to $\vec{\alpha}_b$ and that happens if and only if $\vec{\alpha}_a = \vec{\alpha}_b$. In general, $\vec{\alpha}_a \neq \vec{\alpha}_b$ and we *cannot* conclude that $\mathbf{b}$ is an array manifold at frequency ω_c, because $|\vec{\beta}| < 1/c$. Depending on the array manifold vector, we might be able to find other types of the transformation matrices that satisfy the Lemma 1. At this time, it is not guaranteed that TOPS will work for general 3-D arrays.

When the span of $\{\vec{x}_m\}$ is 2-D or 1-D, however, $\mathbf{b}$ can be defined to be an array manifold at frequency ω_3. For example, consider the2-D case and assume that the sensor positions $\vec{x}_m = [x_m, y_m, z_m]$ all have $z_m = 0$. Then (33) leads to the conclusion that the x and y components of $\vec{\beta}$ must satisfy (34), but the z component is unconstrained. Since $\vec{\beta}$ defined in (34) has a magnitude smaller than $1/c$, we can increase the z component to obtain a legitimate slowness vector. The same logic applies when the span of $\{\vec{x}_m\}$ is 1-D except that now both the y and z components could be increased to satisfy $|\vec{\beta}| = 1/c$.

Therefore, $\mathbf{b}$ is an array manifold and it can be concluded that the TOPS method works with arbitrary 1-D or 2-D arrays unless the array manifolds are linearly dependent, but then any signal subspace method would also fail. Although, TOPS works with arbitrary 1-D or 2-D arrays, only ULAs will be considered in the simulations for convenience. It is straightforward to extend the following discussion to other arrays.

C. Signal Subspace Projection

In practice, the correlation matrices are unavailable, so estimated correlation matrices are used in place of the true correlation. In order to estimate the correlation matrix, the sensor outputs are divided into J blocks, with the number of samples in one block being equal to the number of DFT points. If we let

$\mathbf{x}_{j,i}$ be the sensor DFT output at $\omega = \omega_i$ for the jth block, then the estimated correlation matrix is

$$\hat{\mathbf{R}}_i = \frac{1}{J}\sum_{j=0}^{J-1} \mathbf{x}_{j,i}\mathbf{x}_{j,i}^H. \tag{36}$$

From $\hat{\mathbf{R}}_i$, we can find the signal and noise subspaces $\hat{\mathbf{F}}_i$ and $\hat{\mathbf{W}}_i$. The DOA estimation performance depends on the quality of the estimated correlation matrix which, in turn, is fully determined by the number of snapshots and the SNR, which are not usually under the control of the processor. By subspace projection, however, it is possible to reduce some error terms in the TOPS matrix $\hat{\mathbf{D}}(\phi)$. If we define a projection matrix $\mathbf{P_i}(\theta)$ onto the null space of $\mathbf{a}_i(\phi)$

$$\mathbf{P}_i(\phi) = \mathbf{I} - \left(\mathbf{a}_i^H(\phi)\mathbf{a}_i(\phi)\right)^{-1}\mathbf{a}_i(\phi)\mathbf{a}_i^H(\phi) \tag{37}$$

then we can form a modified $\mathbf{D}(\phi)$ matrix where $\mathbf{U}_i(\phi)$ is replaced by

$$\mathbf{U}_i'(\phi) = \mathbf{P}_i(\phi)\mathbf{U}_i(\phi). \tag{38}$$

This projection can reduce the signal subspace component leakage in the estimated noise subspace. Estimates from this modified $\mathbf{D}(\phi)$ matrix exhibit less mean square error (see Appendix B). Note that this projection method can be used only when the distance between sensors is less than half the wavelength of the highest frequency used in the processing, not the center frequency; otherwise, aliasing occurs.

D. Algorithm

Since both the signal subspace and noise subspace are estimated, it is unlikely that $\mathbf{D}$ would ever become rank deficient. However, we can find how close a matrix is to being rank-deficient by looking at the condition number or the minimum singular value of the matrix [21]. In our case, the smallest singular value is a better choice because we are looking for the case where $\mathbf{D}$ becomes rank deficient when one of its row vectors (49) is a zero vector.

The following steps summarize the TOPS method of finding DOAs of wideband sources for 1-D arrays.

1) Divide the sensor output into J identical sized blocks.
2) Compute the temporal DFT of the J blocks.
3) For the jth block, select $\mathbf{x}_{j,k}$ at preselected ω_k, where $k = 0, \ldots, K-1$ and $j = 0, \ldots, J-1$.
4) Compute the signal subspace $\hat{\mathbf{F}}_1$ and the noise subspace $\hat{\mathbf{W}}_k$ for $k = 1, \ldots, K-1$ by SVD of the estimated covariance matrices $\hat{\mathbf{R}}_k$.
5) Generate $\hat{\mathbf{D}}(\phi)$ using (38) and (28) for each hypothesized DOA ϕ.
6) Estimate $\hat{\theta}$ by

$$\hat{\theta} = \arg\max_{\phi} \frac{1}{\sigma_{\min}(\phi)} \tag{39}$$

where $\sigma_{\min}(\phi)$ is the smallest singular value of $\hat{\mathbf{D}}(\phi)$.

The estimation is now to find P local maxima by doing a one-dimensional search.

E. Computational Complexity

It is not easy to calculate the exact computational cost for TOPS. The number of computations for an $M \times M$ SVD is $O(M^3)$ [21]. The minimum nonzero singular values of the $\mathbf{D}$ matrix can be found via an SVD of a $P \times P$ matrix, so $O(P^3)$ computations have to be done for each hypothesized ϕ. For CSSM or WAVES, once they have formed the coherent correlation matrix, only a single SVD is required to use a typical narrowband signal subspace method. Therefore, those methods require fewer computations than TOPS. However, the process of finding the RSS focusing matrices requires an SVD of an $M \times M (M > 2P)$ matrix for each frequency bin. Thus, if we consider the computational cost for preprocessing and the performance results shown in the following section, TOPS is still a viable alternative choice for wideband DOA estimation.

IV. Simulation

A. Simulation Model

TOPS has been tested through computer simulations by considering a ten-sensor ULA. The statistical performance was evaluated by performing 200 Monte Carlo runs for each scenario. Three far-field uncorrelated wideband sources are placed at 8°, 33°, and 37°, respectively. Two types of wideband sources are used in the simulation: a sinc function with random magnitude, and a sum of sinusoids with random magnitude and random phase, viz.,

$$s(t) = a(t)\sum_{i=1}^{N_f} \exp\{j(2\pi f_i t + c_i)\} \tag{40}$$

where the amplitude $a(t)$ is a Rayleigh random variable and the phase c_i is uniformly distributed in $[-\pi, \pi]$. Note that the signal frequencies $f_1, f_2, \ldots, f_{N_f}$ are different from the frequency bins used in the processing. For both sources, the fractional bandwidth, i.e., the ratio of bandwidth divided by the center frequency, is 2/3. The sampling frequency is three times the highest frequency. In other words, the wideband signal sits between $(1/3)\pi$ and $(2/3)\pi$ in the ω domain. The sensor output was divided into 100 blocks ($J = 100$), and each block has 256 snapshots.

Three other methods were tested for comparison: CSSM, WAVES, and Incoherent MUSIC (IMUSIC) [see (12)]. For the proposed method, seven frequency bins are used while CSSM and WAVES use 22 frequency bins; IMUSIC uses the same seven frequency bins as TOPS. RSS focusing matrices [15] are used to cohere the sample covariance matrices in the two coherent methods. Both CSSM and WAVES are processed once. It means that there was no recursive processing to update focusing angles and weighting matrices.

The sensor spacing is half the wavelength corresponding to the center frequency, not to the highest frequency of the signal [4], [5]. CSSM and WAVES are resilient to aliasing at higher frequencies due to the coherent averaging. It is possible for TOPS to suffer from aliasing when the aliased DOAs fold into true DOAs at all frequency bins. However, this pathological case is very unlikely. It is possible to avoid aliasing by setting the

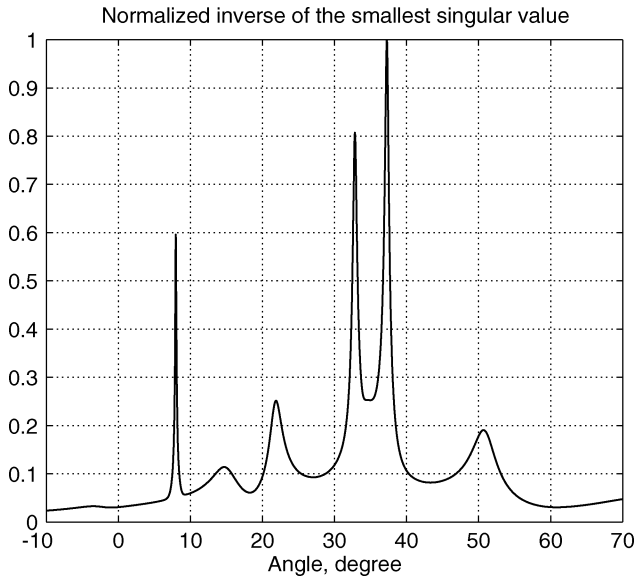

Fig. 1. Example result of the proposed algorithm. The peaks of the normalized condition number indicate three DOAs. The source signal is sinc and SNR is 13 dB for this run.

sensor spacing to be half the shortest wavelength. However, in that case, the length of the array is shorter and the estimator performance would degrade due to poorer resolution.

B. Focusing Angles

For the coherent methods, the focusing angles are one of the most important factors that impact the estimator's performance. In the simulations presented here, two different kinds of focusing angles are used. First, we used perturbations of the true DOAs by adding Gaussian random noise, so we have

$$\boldsymbol{\theta}_F \sim \mathcal{N}\left(\boldsymbol{\theta}, \sigma_f^2 \mathbf{I}\right) \tag{41}$$

as focusing angles. Various values of σ_f were used in the simulations. It should be mentioned here that the errors in focusing angles are usually coupled, so it is a little bit unrealistic to use independent errors between focusing angles. However, simulations with those perturbed focusing angles can give some idea of how much error is tolerable.

The second type of focusing angles used is the focusing strategy in [15], which is much more realistic. That is, 1) find approximate DOAs μ_i using low-resolution algorithms and then 2) use μ_i, $\mu_i + 0.25$ BW, and $\mu_i - 0.25$ BW as focusing angles, where BW denotes the beamwidth. Unlike the focusing angles which are fixed in [15], we use variable μ_i's that are estimated during each run. This seems more natural since the μ_i's are also random variables. Capon's method [22] is employed as the low-resolution algorithm to obtain the estimates μ_i. DOA estimates of multiple frequency bins by Capon are averaged and used in the coherent methods. After focusing, we used ROOT-MUSIC as the narrowband method [23].

C. Results

Fig. 1 shows one example run of TOPS for a ten-sensor ULA. The normalized inverse of the smallest singular value indicates that there are three sources because one can see three sharp peaks at the correct DOAs. Note that the magnitude is not necessarily proportional to the power of the signal sources.

Fig. 2 compares the average estimation results, e.g., bias, standard deviation, and root-mean-squared (rms) error, between CSSM and TOPS for different SNR levels when the sources are multitonal. For the CSSM methods, the focusing angles were determined as a random perturbation for the true DOAs. Different CSSM curves in the figure represent different variances for the perturbation. The figure shows the results for the sources at 33° and 37°. The results for all methods were virtually identical for the isolated source at 8°, and these results are not included.

The results in Fig. 2 show that the performance of CSSM is dominated by errors in focusing angles rather than SNR. As the SNR increases, TOPS shows better performance. When SNR is as high as 25 dB, TOPS begins to demonstrate smaller RMS error than CSSM with focusing errors as small as $0.316^\circ (\sigma_f^2 = 0.1 \text{ degrees}^2)$. It should be noted, however, that the number of runs that could resolve the 33° and 37° sources was smaller for TOPS than for CSSM. When SNR is below 0 dB, TOPS could not resolve the two closest sources. This is an expected result since TOPS is an incoherent method for which the processing gain is much less than coherent methods when SNR is low.

The performance results when using the results of Capon's wideband method for the focusing angles are shown in Fig. 3 for sinc sources. The figure includes results for TOPS, CSSM, WAVES, and IMUSIC. The ability of the wideband Capon method to obtain good focusing angles is now related to the SNR. Therefore, the standard deviation of CSSM and WAVES now decreases more significantly as SNR increases. However, these coherent methods are still biased for high SNR and perform worse than TOPS. At low SNR, the coherent methods are able to provide better estimates than TOPS. Note again that the number of successful runs that could resolve the two closest sources was larger for the coherent methods. Interestingly, IMUSIC exhibits better performance than TOPS in high SNR range, but it could resolve the 33° and 37° sources less than TOPS when the SNR was lower than 3 dB.

TOPS demonstrated better bias but worse standard deviation than the coherent methods in low SNR. The overall performance for CSSM and WAVES were very similar.

IMUSIC exhibited the worst biases among all four methods in the low SNR range. As SNR increases, however, both the bias and standard deviation of IMUSIC decreases, and at high SNR, it outperforms the other methods. TOPS exhibited higher standard deviation than IMUSIC. The coherent methods outperformed the incoherent methods in terms of the number of runs that resolve two close targets as well as the standard deviation at low SNR.

Fig. 3(e) and (f) summarizes the estimator's performance by showing the RMS error. It shows the mutual advantages of each method over SNR range. TOPS exhibited the average performance in the whole SNR in terms of rms error while IMUSIC was best in midto high SNR and the coherent methods were best in low SNR. We should mention here again that it seems that the performance of WAVES and CSSM is dominated by the quality

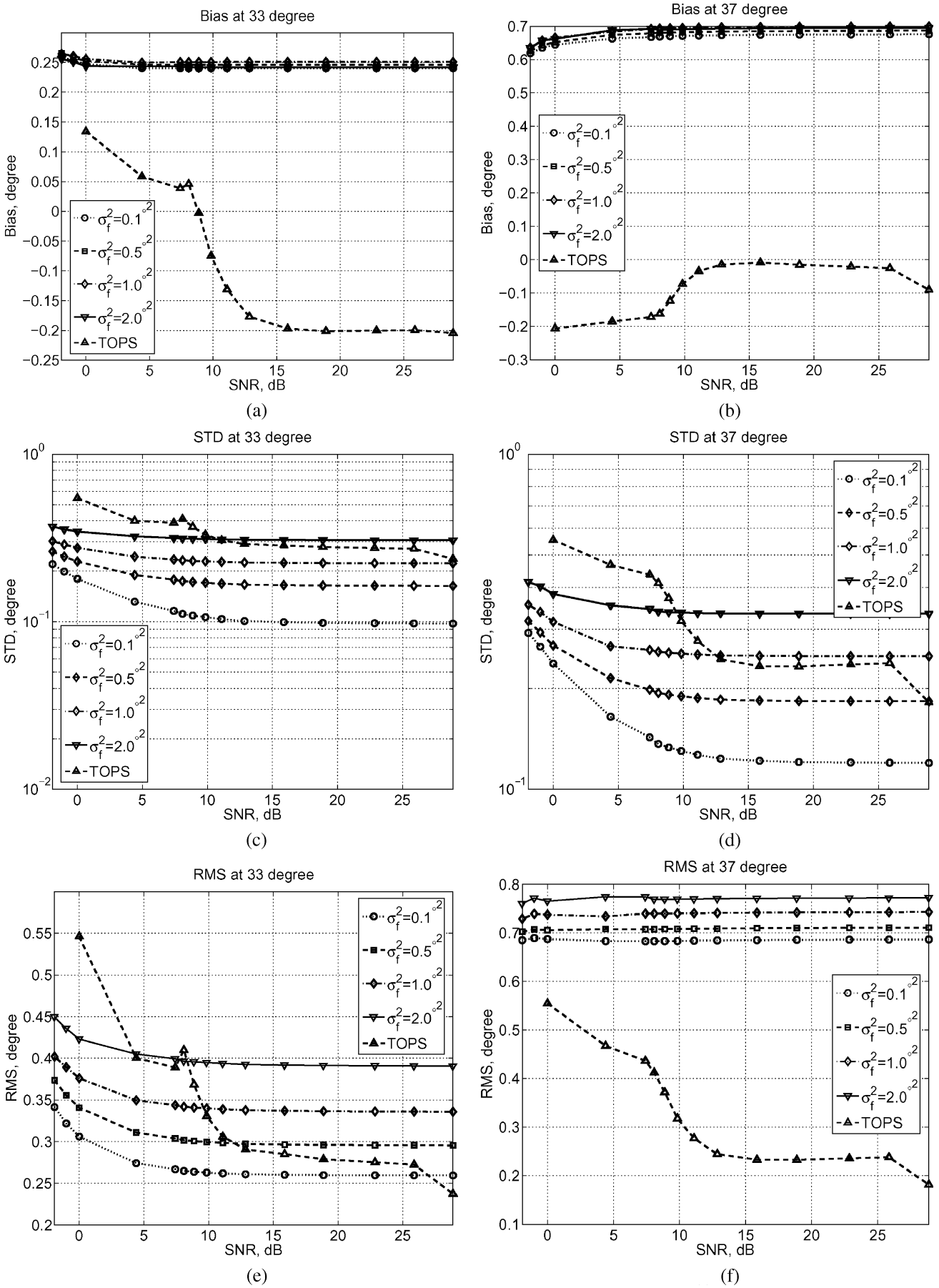

Fig. 2. Comparison of estimation performance between CSSM using random DOA initializations and TOPS where the sources are multitonal: (a) bias for the source at 33°; (b) bias for the source at 37°; (c) standard deviation for source at 33°; (d) standard deviation of source at 37°; (e) rms error for source at 33°; and (f) rms error for source at 37°.

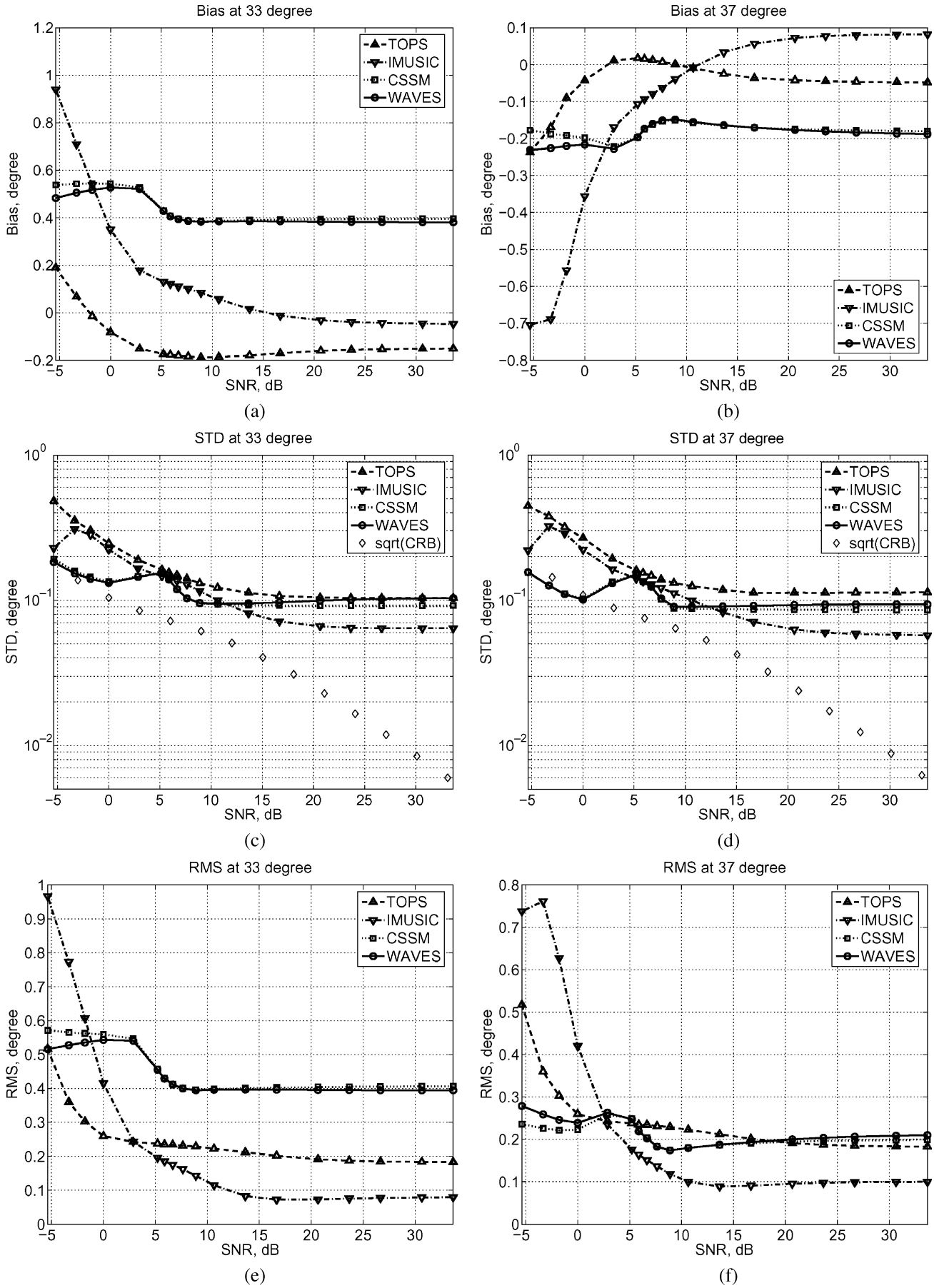

Fig. 3. Estimation performance for the different wideband algorithms using Capon method for initial DOAs where the sources are sincs: (a) bias for the source at 33°; (b) bias for the source at 37°; (c) standard deviation for source at 33°; (d) standard deviation of source at 37°; (e) rms error for source at 33°; and (f) rms error for source at 37°.

of the initial focusing angles. The results for CSSM and WAVES when using the Capon method for initialization provides a realistic representation of the focusing error. If it were possible for the focusing angles to be smaller in these simulations, the performance of the coherent method would become better than that of TOPS or IMUSIC.

V. Conclusion

We have proposed a new wideband DOA estimator, TOPS, which exploits the signal and noise subspaces of multiple frequency bins. This method is different from the usual incoherent methods since it takes advantage of subspaces from multiple frequencies simultaneously. It is also different from coherent methods that form a general coherent correlation matrix using focusing angles. We have shown that the performance of TOPS sits between incoherent and coherent methods, and the simulation showed that the performance of TOPS is between that of the coherent and the incoherent methods in the whole SNR range while coherent methods work best in low SNR, and IMUSIC works best at high SNRs. Another advantage of TOPS is that it uses both the signal and the noise subspaces estimated from the data. Previous methods use an analytical form of the array manifold to find DOAs, so the bandpass filtering effect of the DFT is not considered. The output of a bandpass filter is usually not a perfect narrowband signal. The bandwidth of those filtered signals could degrade the estimator's performance even in the high SNR case. Since TOPS uses the signal subspace of data and transforms only the array manifold of the desired frequency, it should reduce those degradations. We believe that TOPS represents a new way of processing multiple subspaces and would be able to improve DOA estimates not only for wideband sources but also for acoustic sources having multiple harmonics. We also believe that we could improve the performance of TOPS by using weighted subspaces similar to weighted subspace fitting (WSF) [19].

Appendix A
Proof of Theorem 1

The theorem says that $\phi = \theta_l$ for some l is the only case where the $\mathbf{D}(\phi)$ becomes rank deficient. The statements a and b should be proven independently.

Proof of a: Let ϕ be equal to the lth DOA θ_l. Since $\mathbf{W}_i$ is the noise subspace, $\mathbf{A}_i^H\mathbf{W}_i = \mathbf{0}_{[P\times(M-P)]}$. Therefore,

$$\mathbf{a}_i^H(\theta_l)\mathbf{W}_i = \mathbf{0}^T \tag{42}$$

for all $l = 0, 1, \ldots, P-1$ and $i = 0, 1, \ldots, K-1$. By Lemma 2, we know that

$$\mathbf{U}_i = \mathbf{\Phi}(\Delta\omega_i, \phi)\mathbf{A}_0\mathbf{G}_0 = \mathbf{A}_i(\hat{\boldsymbol{\theta}}_i)\mathbf{G}_0 \tag{43}$$

where

$$[\hat{\boldsymbol{\theta}}_i]_p = \arcsin\left\{\frac{\omega_1}{\omega_i}\sin\theta_p + \frac{\Delta\omega_i}{\omega_i}\sin\phi\right\} \tag{44}$$

for $p = 0, 1, \ldots, P-1$. Since $\phi = \theta_l$

$$[\hat{\boldsymbol{\theta}}_1]_l = \ldots = [\hat{\boldsymbol{\theta}}_{K-1}]_l = \theta_l. \tag{45}$$

Therefore

$$\begin{aligned}\mathbf{U}_i^H\mathbf{W}_i &= \mathbf{G}_0^H\begin{bmatrix}\mathbf{a}_i^H(\hat{\theta}_0)\mathbf{W}_i\\ \vdots\\ \mathbf{a}_i^H(\theta_l)\mathbf{W}_i\\ \vdots\\ \mathbf{a}_i^H(\hat{\theta}_{P-1})\mathbf{W}_i\end{bmatrix}\\ &= \mathbf{G}_0^H\begin{bmatrix}\vdots\\ \mathbf{0}^T\\ \vdots\end{bmatrix} \leftarrow l\text{th row.}\end{aligned} \tag{46}$$

Then, the $\mathbf{D}$ matrix becomes

$$\begin{aligned}\mathbf{D} &= \left[\mathbf{U}_1^H\mathbf{W}_1 \ldots \mathbf{U}_{K-1}^H\mathbf{W}_{K-1}\right]\\ &= \mathbf{G}_0^H\begin{bmatrix}\vdots & \cdots & \vdots\\ \mathbf{0}^T & \cdots & \mathbf{0}^T\\ \vdots & \cdots & \vdots\end{bmatrix} \leftarrow l\text{th row}\end{aligned} \tag{47}$$

and it loses rank. This proves that $\phi = \theta_l$ is a sufficient condition for $\mathbf{D}$ to become rank deficient.

Proof of b: Suppose that the $\mathbf{D}$ matrix is rank deficient. Since $\mathbf{D}$ has more columns than rows, the rows must be linearly dependent. Using (26) and (27), the expression for $\mathbf{D}(\phi)$ can be rewritten as

$$\mathbf{D}(\phi) = \mathbf{G}_0^H\mathbf{L} \tag{48}$$

where

$$\mathbf{L} = [\mathbf{L}_1 \ \cdots \ \mathbf{L}_{K-1}] \tag{49}$$

and $\mathbf{L}_i = \mathbf{A}_i^H(\hat{\boldsymbol{\theta}}_i)\mathbf{W}_i$. Because $\mathbf{G}_0$ is a nonsingular square matrix, the row vectors of $\mathbf{L}$ are also linearly dependent.

There are two cases that we need to consider. The first case is when all $\hat{\theta}$'s are different from the DOAs; the other is when some of the $\hat{\theta}$'s are the same as the DOAs. Since these two cases work out differently depending on whether the individual block matrices $\mathbf{L}_i$'s are full rank or not, we need to consider both cases independently.

Case I: Assume that all the $\hat{\theta}$'s are different from the DOAs. Then there is no zero row vector in $\mathbf{L}_i$. With slight abuse of the notation, let $\hat{\mathbf{A}}_i = \mathbf{A}_i(\hat{\boldsymbol{\theta}}_i)$ and $\mathbf{A}_i = \mathbf{A}_i(\boldsymbol{\theta}_i)$. Define $\mathbf{B}$ and $\mathbf{C}$ as

$$\mathbf{B} = [\mathbf{A}_i \quad \hat{\mathbf{A}}_i] \tag{50}$$

and

$$\mathbf{C} = [\mathbf{A}_i \quad \mathbf{W}_i]. \tag{51}$$

Since $P < M/2$, the rank of $\mathbf{B}$ is $2P$, and the rank of $\mathbf{C}$ is M, and the product $\mathbf{B}^H\mathbf{C}$ is

$$\mathbf{B}^H\mathbf{C} = \begin{bmatrix} \mathbf{A}_i^H \\ \hat{\mathbf{A}}_i^H \end{bmatrix} [\mathbf{A}_i \quad \mathbf{W}_i] = \begin{bmatrix} \mathbf{A}_i^H\mathbf{A}_i & \mathbf{0} \\ \hat{\mathbf{A}}_i^H\mathbf{A}_i & \mathbf{L}_i \end{bmatrix}. \tag{52}$$

Sylvester's inequality states that the rank of $\mathbf{B}^H\mathbf{C}$ should be bounded by [24]

$$\gamma(\mathbf{B}) + \gamma(\mathbf{C}) - M \le \gamma(\mathbf{B}^H\mathbf{C}) \le \min(\gamma(\mathbf{B}), \gamma(\mathbf{C})) \tag{53}$$

where $\gamma(\cdot)$ denotes rank of a matrix. Therefore

$$2P \le \gamma(\mathbf{B}^H\mathbf{C}) \le 2P. \tag{54}$$

In other words, $\mathbf{B}^H\mathbf{C}$ is always full rank. Since the upper right block is a zero matrix, $\mathbf{L}_i$ is always full rank and the row vectors in $\mathbf{L}_i$ are linearly independent for all i, because $\mathbf{L}_i$ has more columns than rows. This proves the nonsingularity of $\mathbf{L}$. Therefore, Case I does not happen. Note that for the case where $2P > M$, we cannot guarantee that $\mathbf{L}$ still has independent rows.

Case II: From the proof of Case I, it is known that when $\mathbf{D}(\phi)$ is rank deficient some of the $\hat{\theta}$'s are the same as the DOAs, so that the corresponding $\mathbf{L}_i$ is also rank deficient. Of course, this happens when the hypothesized ϕ is the same as one of the DOAs. However, in the multiple-source case, there is ambiguity when $\hat{\theta}$ happens to be the same as one of the DOAs, even if the hypothesized ϕ does not match any of the DOAs. For example, let $[\hat{\boldsymbol{\theta}}_k]_l$ be the lth DOA of $\hat{\mathbf{A}}_k$. Even if ϕ is not equal to any of the θ_i, it is possible that, for $l \neq i$, $[\hat{\boldsymbol{\theta}}_k]_l = \theta_i$ where

$$[\hat{\boldsymbol{\theta}}_k]_l = \arcsin\left\{ \frac{\omega_1}{\omega_k}\sin\theta_l + \frac{\omega_k - \omega_1}{\omega_k}\sin\phi \right\}. \tag{55}$$

In this case, $\mathbf{L}_k$ loses its rank since its lth row will be zero. Note that it is the only case where $\mathbf{L}_k$ becomes rank deficient. Otherwise, $\mathbf{L}_k$ can be shown to be full rank following the same steps as in the proof of Case I. Without loss of generality, let's assume that $[\hat{\boldsymbol{\theta}}_1]_l = \theta_i$. Then, $\mathbf{e}_l^H\mathbf{L}_1 = \mathbf{0}^T$, where $\mathbf{e}_l$ is a vector whose elements are zero except for the lth element, which is one. Any null space of $\mathbf{L}_k$ can be spanned by $\mathbf{e}_l$. If $\mathbf{L}$ is rank deficient

$$\bigcap_{k=1}^{K-1} \mathcal{N}\{\mathbf{L}_k\} \neq \emptyset. \tag{56}$$

Since the $\mathbf{e}_l$'s form an orthogonal set, (56) is equivalent to the fact that there exists one $\mathbf{e}_l$ such that $\mathbf{e}_l^H\mathbf{L}_k = \mathbf{0}^T$ for all $k = 1, \ldots, K-1$, implying that $\hat{\theta}_l^{(k)} = \theta_i$ for all k. Since the right-hand side of (55) is monotonically increasing or decreasing, we conclude that $\hat{\theta}_l^{(k)} \neq \hat{\theta}_l^{(j)}$ as long as $k \neq j$. Since it is assumed that $\phi \neq \theta_l$, $\hat{\theta}_l^{(k)} \neq \theta_l$, and $\hat{\theta}^{(k)}$ can be the same as one of the DOAs at most $P-1$ times. Therefore, if $K-1 > P$, there does not exist $\mathbf{e}_l$ such that $\mathbf{e}_l^H\mathbf{L}_k = \mathbf{0}^T$ for all $k = 1, \ldots, K$ and $\mathbf{L}$ is nonsingular as long as $\phi \neq \theta_i$ for all i. We can conclude that $\mathbf{D}(\phi)$ is rank-deficient if and only if $\phi = \theta_i$ for some i.

APPENDIX B
SUBSPACE PROJECTION

Let $\hat{\mathbf{F}}_i$ and $\hat{\mathbf{W}}_i$ be the estimated signal and noise subspace matrices, respectively. We can represent these estimated matrices, including perturbations, as

$$\hat{\mathbf{F}}_i = \bar{\mathbf{F}}_i + \delta\mathbf{F}_i$$
$$\hat{\mathbf{W}}_i = \bar{\mathbf{W}}_i + \delta\mathbf{W}_i$$

where $\bar{\mathbf{F}}_i$ and $\bar{\mathbf{W}}_i$ are in the range of $\mathbf{F}_i$ and $\mathbf{W}_i$, respectively. The error matrices $\delta\mathbf{F}_i$ and $\delta\mathbf{W}_i$ satisfy

$$\delta\mathbf{F}_i \subset \mathcal{N}\{\mathbf{F}_i\}$$
$$\delta\mathbf{W}_i \subset \mathcal{R}\{\mathbf{F}_i\}$$

and if the number of samples is large, it can be assumed that the error matrices are small in the Frobenius norm, i.e., $\|\delta\mathbf{F}\|_F \ll \|\mathbf{F}\|_F$ and $\|\delta\mathbf{W}\|_F \ll \|\mathbf{W}\|_F$. Let $\boldsymbol{\Phi}_i = \boldsymbol{\Phi}(\Delta\omega_i, \phi)$. When $\phi = \theta_l$,

$$\begin{aligned} \hat{\mathbf{F}}_0^H\boldsymbol{\Phi}_i^H\hat{\mathbf{W}}_i &= \left(\bar{\mathbf{F}}_0^H + \delta\mathbf{F}_0^H\right)\boldsymbol{\Phi}_i^H(\bar{\mathbf{W}}_i + \delta\mathbf{W}_i) \\ &\approx \bar{\mathbf{F}}_0^H\boldsymbol{\Phi}_i^H\bar{\mathbf{W}}_i + \delta\mathbf{F}_0^H\boldsymbol{\Phi}_i^H\bar{\mathbf{W}}_i + \bar{\mathbf{F}}_0^H\boldsymbol{\Phi}_i^H\delta\mathbf{W}_i \\ &\simeq \bar{\mathbf{G}}_0^H\begin{bmatrix} \vdots \\ \mathbf{0}^T \\ \vdots \end{bmatrix} + \delta\mathbf{F}_0^H\boldsymbol{\Phi}_i^H\bar{\mathbf{W}}_i + \bar{\mathbf{F}}_0^H\boldsymbol{\Phi}_i^H\delta\mathbf{W}_i \end{aligned} \tag{57}$$

where $\bar{\mathbf{G}}_0$ is in the range of $\mathbf{G}_0$. Note that the second-order term is neglected above in the second line. The terms other than the first term prevent $\hat{\mathbf{F}}_0^H\boldsymbol{\Phi}_i^H\hat{\mathbf{W}}_i^H$ from losing rank. When the projection matrix $\mathbf{P}_i$ is included, the second term in (57) is unchanged since $\mathbf{P}_i^H = \mathbf{P}_i$ and $\mathbf{P}_i\bar{\mathbf{W}}_i = \bar{\mathbf{W}}_i$. In other words

$$\delta\mathbf{F}_0^H\boldsymbol{\Phi}_i^H\mathbf{P}_i^H\bar{\mathbf{W}}_i = \delta\mathbf{F}_0^H\boldsymbol{\Phi}_i^H\bar{\mathbf{W}}_i. \tag{58}$$

The third term becomes

$$\bar{\mathbf{F}}_0^H\boldsymbol{\Phi}_i^H\mathbf{P}_i^H\delta\mathbf{W}_i = \bar{\mathbf{G}}_0^H\begin{bmatrix} \vdots \\ \mathbf{0}^T \\ \vdots \end{bmatrix}. \tag{59}$$

The projection matrix removes the array manifold $\mathbf{a}_i(\theta_l)$ that might be included in $\delta\mathbf{W}_i$.

Then

$$\hat{\mathbf{F}}_0^H \mathbf{\Phi}_i^H \mathbf{P}_i^H \hat{\mathbf{W}}_i \simeq \bar{\mathbf{G}}_0^H \begin{bmatrix} \vdots \\ \mathbf{0}^T \\ \vdots \end{bmatrix} + \delta \mathbf{F}_0^H \mathbf{\Phi}_i^H \bar{\mathbf{W}}_i + \bar{\mathbf{G}}_0^H \begin{bmatrix} \vdots \\ \mathbf{0}^T \\ \vdots \end{bmatrix}$$

$$\simeq \bar{\mathbf{G}}_0^H \begin{bmatrix} \vdots \\ \mathbf{0}^T \\ \vdots \end{bmatrix} + \delta \mathbf{F}_0^H \mathbf{\Phi}_i^H \bar{\mathbf{W}}_i. \quad (60)$$

The error term is reduced by one term and this gives less perturbation on the smallest singular value.

REFERENCES

[1] H. Krim and M. Viberg, "Two decades of array signal processing research: The parametric approach," *IEEE Signal Process. Mag.*, vol. 13, no. 4, pp. 67–94, Jul. 1996.

[2] D. Lake, "Harmonic phase coupling for battlefield acoustic target identification," presented at the *Proc. IEEE Acoustics, Speech, Signal Processing (ICASSP)*, Seattle, WA, May 1998.

[3] R. Schmidt, "Multiple emitter location and signal parameter estimation," *IEEE Trans. Antennas Propag.*, vol. AP-34, no. 3, pp. 276–280, Mar. 1986.

[4] H. Wang and M. Kaveh, "Coherent signal-subspace processing for the detection and estimation of angles of arrival of multiple wideband sources," *IEEE Trans. Acoust., Speech, Signal Process.*, vol. ASSP-33, no. 4, pp. 823–831, Aug. 1985.

[5] E. Di Claudio and R. Parisi, "WAVES: Weighted average of signal subspaces for robust wideband direction finding," *IEEE Trans. Signal Process.*, vol. 49, no. 10, pp. 2179–2190, Oct. 2001.

[6] M. Doron and E. Doron, "Wavefield modeling and array processing, Part II—Algorithms," *IEEE Trans. Signal Processing*, vol. 42, no. 10, pp. 2560–2570, Oct. 1994.

[7] B. Friedlander and A. Weiss, "Direction finding of wideband signals using an interpolated array," *IEEE Trans. Signal Process.*, vol. 41, no. 4, pp. 1618–1634, Apr. 1993.

[8] T.-S. Lee, "Efficient wideband source localization using beamforming invariance technique," *IEEE Trans. Signal Process.*, vol. 42, no. 6, pp. 1376–1387, Jun. 1994.

[9] S. Valaee and P. Kabal, "Wideband array processing using a two-sided correlation transformation," *IEEE Trans. Signal Process.*, vol. 43, no. 1, pp. 160–172, Jan. 1995.

[10] T. Pham and B. Sadler, "Adaptive wideband aeroacoustic array processing," *Proc. 8th IEEE Signal Processing Workshop Statistical Signal Array Processing*, pp. 295–298, Jun. 1996.

[11] D. Swingler and J. Krolik, "Source location bias in the coherently focused high-resolution broadband beamformer," *IEEE Trans. Acoust., Speech, Signal Process.*, vol. 37, no. 1, pp. 143–145, Jan. 1989.

[12] M. Wax and T. Kailath, "Determining the number of signals by information theoretical criteria," in *Proc. ASSP Spectrum Estimation Workshop II*, Tampa, FL, 1983, pp. 192–196.

[13] ——, "Spatio-temporal spectral analysis by eigenstructure methods," *IEEE Trans. Acoust., Speech, Signal Process.*, vol. ASSP-32, no. 4, pp. 817–827, Aug. 1984.

[14] H. Hung and M. Kaveh, "Coherent wideband ESPRIT method for direction-of-arrival estimation of multiple wideband sources," *IEEE Trans. Acoust., Speech, Signal Process.*, vol. 38, no. 2, pp. 354–356, Feb. 1990.

[15] ——, "Focusing matrices for coherent signal-subspace processing," *IEEE Trans. Acoust., Speech, Signal Process.*, vol. ASSP-36, no. 8, pp. 1272–1282, Aug. 1988.

[16] M. Doron and A. Weiss, "On focusing matrices for wideband array processing," *IEEE Trans. Signal Process.*, vol. 40, no. 6, pp. 1295–1302, Jun. 1992.

[17] J. Krolik, "Focused wideband array processing for spatial spectral estimation," in *Advances in Spectrum Analysis and Array Processing, Vol. II*, S. Haykin, Ed. Englewood Cliffs, NJ: Prentice-Hall, 1991, ch. 6.

[18] M. Doron and E. Doron, "Wavefield modeling and array processing, Part I—Spatial sampling," *IEEE Trans. Signal Process.*, vol. 42, no. 10, pp. 2549–2559, Oct. 1994.

[19] M. Viberg, B. Ottersten, and T. Kailath, "Detection and estimation in sensor arrays using weighted subspace fitting," *IEEE Trans. Signal Process.*, vol. 39, no. 11, pp. 2436–2449, Nov. 1991.

[20] D. Johnson and D. Dudgeon, *Array Signal Processing: Concepts and Techniques*. Englewood Cliffs, NJ: Prentice-Hall, 1993.

[21] G. Golub and C. VanLoan, *Matrix Computations*. Baltimore, MD: The Johns Hopkins Univ. Press, 1996.

[22] J. Capon, "High-resolution frequency-wavenumber spectrum analysis," *Proc. IEEE*, vol. 57, Aug. 1969.

[23] A. Barabell, "Improving the resolution performance of eigen-structure-based direction-finding algorithms," in *Proc. Int. Conf. Acoustics, Speech, Signal Processing (ICASSP)*, 1983, pp. 336–339.

[24] C.-T. Chen, *Linear System Theory and Design*. New York: Oxford Univ. Press, 1984.

[25] M. Kaveh and A. Barabell, "The statistical performance of the MUSIC and the minimum-norm algorithms in resolving plane waves in noise," *IEEE Trans. Acoust., Speech, Signal Process.*, vol. ASSP-34, no. 2, pp. 331–341, Apr. 1986.

[26] P. Stoica and A. Nehorai, "MUSIC, maximum likelihood, and cramer-rao bound," *IEEE Trans. Acoust., Speech, Signal Process.*, vol. 37, no. 5, pp. 720–741, May 1989.

[27] B. Ottersten and T. Kailath, "Direction-of-arrival estimation for wideband signals using the ESPRIT algorithm," *IEEE Trans. Acoust., Speech, Signal Process.*, vol. ASSP-38, pp. 317–327, Feb. 1990.

[28] R. Roy and T. Kailath, "ESPRIT-estimation of signal parameters via rotational invariance techniques," *IEEE Trans. Signal Process.*, vol. 37, no. 7, pp. 984–995, Jul. 1989.

[29] Y.-S. Yoon, L. Kaplan, and J. McClellan, "New signal subspace direction-of-arrival estimator for wideband sources," presented at the IEEE Acoustics, Speech, Signal Processing (ICASSP), Hong Kong, Apr. 2003.

[30] ——, "Direction-of-arrival estimation of wideband sources using arbitrary shaped multidimensional arrays," presented at the IEEE Acoustics, Speech, Signal Processing (ICASSP), Montreal, QC, Canada, May 2004.

[31] H. V. Trees, *Optimum Array Processing*. New York: Wiley, 2002.

Yeo-Sun Yoon (S'02–M'05) received the B.S. degree from Yonsei University, Seoul, Korea, in 1995 and the M.S. degree from the University of Michigan, Ann Arbor, in 1998 and the Ph.D. degree from the Georgia Institute of Technology, Atlanta, in 2004, all in electrical engineering.

From 1999 to 2004, he was a Graduate Research Assistant in the Center for Signal and Image Processing (CSIP) at the Georgia Institute of Technology. In the summer, from 2000 to 2002, he worked as a Research Assistant at the Center for Theoretical Studies of Physical Systems (CTSPS), Atlanta, in a co-op program. He currently is a Senior Engineer at the Samsung Thales Company, Ltd., Yongin, Korea. His research interests include array signal processing, signal parameter estimation, and radar signal processing for tracking.

Lance M. Kaplan (S'88–M'89–SM'03) received the B.S. degree with distinction from Duke University, Durham, NC, in 1989 and the M.S. and Ph.D. degrees from the University of Southern California (USC), Los Angeles, in 1991 and 1994, respectively, all in electrical engineering.

From 1987 to 1990, he worked as a Technical Assistant at the Georgia Institute of Technology Research Institute, Atlanta. He held a National Science Foundation Graduate Fellowship and a USC Dean's Merit Fellowship from 1990 to 1993 and worked as a Research Assistant in the Signal and Image Processing Institute at USC from 1993 to 1994. He then worked on staff in the Reconnaissance Systems Department of the Hughes Aircraft Company from 1994 to 1996. From 1996 to 2004, he served on the faculty of the Department of Engineering and the Center for Theoretical Studies of Physical Systems (CTSPS), Clark Atlanta University, Atlanta, GA. Currently, he is a team leader in the EO/IR Image Processing Branch of the U.S. Army Research Laboratory, Adelphi, MD. His current research interests include signal and image processing, data fusion, automatic target recognition, modeling and synthesis, and multiresolution analysis.

Dr. Kaplan serves as Associate Editor-in-Chief and EO/IR Systems Editor for the IEEE TRANSACTIONS ON AEROSPACE AND ELECTRONIC SYSTEMS. He is a three-time recipient of the Clark Atlanta University Electrical Engineering Instructional Excellence Award from 1999 to 2001.

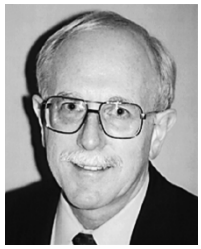

James H. McClellan (S'69–M'74–SM'79–F'85) received the B.S. degree in electrical engineering from Louisiana State University, Baton Rouge, in 1969 and the M.S. and Ph.D. degrees from Rice University, Houston, TX, in 1972 and 1973, respectively.

From 1973 to 1982, he was a Member of the Research Staff and then a Professor with the Lincoln Laboratory, Massachusetts Institute of Technology (MIT), Lexington. From 1982 to 1987, he was with Schlumberger Well Services. Since 1987, he has been a Professor with the School of Electrical and Computer Engineering, Georgia Institute of Technology (Georgia Tech), Atlanta, where he presently holds the John and Marilou McCarty Chair. He is a coauthor of the texts *Number Theory in Digital Signal Processing*, *Computer Exercises for Signal Processing*, *DSP First: A Multimedia Approach*, and *Signal Processing First*, which received the McGraw-Hill Jacob Millman award for an innovative textbook in 2003.

Prof. McClellan received the W. Howard Ector Outstanding Teacher Award from Georgia Tech in 1998 and, in 2001, the Education Award from the IEEE Signal Processing Society. In 1987, he received the Technical Achievement Award for work on FIR filter design, and in 1996, the Society Award, both from the IEEE Signal Processing Society. In 2004, he was a corecipient of the IEEE Jack S. Kilby Signal Processing medal. He is a member of Tau Beta Pi and Eta Kappa Nu.